Maximizing the physics potential of $B^{\pm} \to \pi^{\pm}\mu^{+}\mu^{-}$ decays

Alexander Mclean Marshall,[1,*] Michael Andrew McCann,[2,†] Mitesh Patel,[2,‡] Konstantinos A. Petridis,[1,§] Méril Reboud,[3,4,‖] and Danny van Dyk[3,¶]

[1]H.H. Wills Physics Laboratory, University of Bristol, Bristol, BS8 1TL, United Kingdom
[2]Blackett Laboratory, Imperial College London, London, SW7 2BW, United Kingdom
[3]Institute for Particle Physics Phenomenology and Department of Physics, Durham University, Durham, DH1 3LE, United Kingdom
[4]Physik Department, Universität Siegen, Walter-Flex-Straße 3, 57068 Siegen, Germany

(Received 8 December 2023; accepted 9 May 2024; published 12 June 2024)

We present a method that maximizes the experimental sensitivity to new physics contributions in $B^{\pm} \to \pi^{\pm}\mu^{+}\mu^{-}$ decays. This method relies on performing an unbinned maximum likelihood fit to both the measured dimuon q^2 distribution of $B^{\pm} \to \pi^{\pm}\mu^{+}\mu^{-}$ decays, and theory calculations at spacelike q^2, where QCD predictions are most reliable. Using known properties of the decay amplitude we employ a dispersion relation to describe the nonlocal hadronic contributions across spacelike and timelike q^2 regions. The fit stability and the sensitivity to new physics couplings and new sources of CP-violation are studied for current and future data-taking scenarios, with the LHCb experiment as an example. The proposed method offers a precise and reliable way to search for new physics in these decays.

DOI: 10.1103/PhysRevD.109.116013

I. INTRODUCTION

Over the past decade, several experimental results have hinted at the possibility of new physics in $b \to s\ell^{+}\ell^{-}$ transitions. Most notably, deviations from the predictions of the Standard Model have been observed in the decay rates of $B^0 \to K^{*0}\mu^{+}\mu^{-}$, $B^{\pm} \to K^{*\pm}\mu^{+}\mu^{-}$, $B^{\pm} \to K^{\pm}\mu^{+}\mu^{-}$, and $B_s^0 \to \phi\mu^{+}\mu^{-}$ decays [1–6]; and angular distributions of $B^0 \to K^{*0}\mu^{+}\mu^{-}$, $B^{\pm} \to K^{*\pm}\mu^{+}\mu^{-}$, and $B_s^0 \to \phi\mu^{+}\mu^{-}$ transitions [7–12]. The signs of electron-muon universality violation in $b \to s\ell^{+}\ell^{-}$ have all but evaporated as presented by the recent updates to R_K and R_{K^*} measurements by the LHCb collaboration [13]. This suggests that the decay rates and angular distributions of $b \to se^{+}e^{-}$ processes exhibit the same tensions with SM predictions as their muon counterparts.

Global analyses of these updated measurements point predominantly to anomalous couplings between a left-handed $\bar{s}b$ current and a vectorial lepton current [14,15]. Such a hint is quantitatively supported by, separately, branching ratios and angular $b \to s$ data [16], whose systematic uncertainties are generally very different. A more mundane explanation of the experimental measurements involves underestimating hadronic contributions in the SM [15]. Such hadronic effects involve nonlocal matrix elements of four-quark operators that are hard to compute from first principles. However, recent reappraisals of these hadronic components suggest they are less likely to be the cause of the observed anomalies in $b \to s\mu^{+}\mu^{-}$ decays [17]. Such a conclusion could be validated by suitable observables at high q^2, which share the very same short-distance sensitivity while not suffering from the same long-distance issues [16]. These observables include $B_s \to \mu^{+}\mu^{-}\gamma$ [18] and the inclusive $B \to Xs\mu^{+}\mu^{-}$ [19] among the others.

Traditionally, measurements of $b \to s\mu^{+}\mu^{-}$ transitions involve binning the data in regions of the invariant mass of the dimuon system squared (q^2) and performing measurements of decay rates and angular observables within each of these bins. Recent developments in theory and experiment have opened up the possibility of fitting the entirety of the differential decay rate of $B \to K^{(*)}\mu^{+}\mu^{-}$ transitions to determine new physics couplings and hadronic contributions from the data [20–22].

The additional Cabibbo–Kobayashi–Maskawa (CKM) matrix suppression in the SM of $b \to d\ell^{+}\ell^{-}$ relative to $b \to s\ell^{+}\ell^{-}$ processes makes observables of the former even more sensitive probes of new physics [23]. In light of the tensions with SM predictions in $b \to s\ell^{+}\ell^{-}$ processes,

*alex.marshall@cern.ch
†m.mccann@imperial.ac.uk
‡mitesh.patel@imperial.ac.uk
§konstantinos.petridis@bristol.ac.uk
‖merilreboud@gmail.com
¶danny.van.dyk@gmail.com

maximizing the experimental sensitivity in $B^\pm \to \pi^\pm \mu^+ \mu^-$ decays is of paramount importance to ascertain a more complete picture of the flavor structure of these tensions, be they due to new physics or hadronic effects. Recently, branching fraction measurements of $B^\pm \to \pi^\pm \mu^+ \mu^-$ [24], $B_s^0 \to \bar{K}^{*0} \mu^+ \mu^-$ [25], and $B^0 \to \mu^+ \mu^-$ [26,27] decays have been combined to constrain new physics contributions in $b \to d\ell^+ \ell^-$ processes [28,29]. However, such analyses suffer from limited experimental precision and coarse information regarding the q^2 distribution of $B^\pm \to \pi^\pm \mu^+ \mu^-$ processes. The analysis of Ref. [30] uses a dispersive model for the nonlocal contributions in $b \to d\ell^+ \ell^-$ transitions to predict lepton flavor universality ratios, for which hadronic uncertainties largely cancel. However, in order to ascertain new physics contributions in lepton-flavor-specific final states, it is imperative to separate long- and short-distance effects. This can only be done through an unbinned fit to the dimuon spectrum of $B^\pm \to \pi^\pm \mu^+ \mu^-$ transitions adopting an effective field theory description of the decay amplitudes. Additionally, as will be demonstrated, employing QCD factorization and light-cone sum rules (LCSR) predictions at negative q^2 to constrain the size of hadronic contributions is essential to maximize sensitivity to new physics in these decays, the incorporation of this information is the primary innovation of this paper.

This paper is organized as follows: Sec. II introduces the theoretical background and provides a description of the model used, Sec. III describes how the fits to pseudodatasets are set up, Sec. IV details our results, and finally Sec. V provides a conclusion.

II. THEORETICAL FRAMEWORK

We work within the usual weak effective theory for low-energy $b \to d\ell^+ \ell^-$ transitions. Its effective Lagrangian reads [31,32]

$$\mathcal{L}_{\text{eff}}^{bd\ell\ell} = \frac{4G_F}{\sqrt{2}} (\lambda_c \mathcal{L}_{\text{eff}}^{(c)} + \lambda_u \mathcal{L}_{\text{eff}}^{(u)}) + \text{H.c.}, \tag{2.1}$$

where we abbreviate the CKM factors $\lambda_q = V_{qb} V_{qd}^*$ and use

$$\mathcal{L}_{\text{eff}}^{(p)} = \mathcal{C}_1 \mathcal{O}_1^p + \mathcal{C}_2 \mathcal{O}_2^p + \sum_{i \in \mathcal{I}} \mathcal{C}_i \mathcal{O}_i. \tag{2.2}$$

Above, the sums run over the set of operators $\mathcal{I} = \{3\text{–}10, 7' - 10', P, P', S, S', T, T5\}$. These operators are commonly classified as either semileptonic $(9, 9', 10, 10', P, P', S, S', T, T5)$, radiative $(7, 7', 8, 8')$, current-current $(1, 2)$, and QCD penguin operators (3–6). In contrast to $b \to s$ transitions, $b \to d$ transitions exhibit a flat hierarchy of the CKM factors $\lambda_u \sim \lambda_c \sim \lambda_t$, which requires one to keep all the terms in Eq. (2.1) in the calculations. Note that we allow for BSM physics to enter the weak effective theory through the semileptonic operators $\mathcal{O}_i$ with $i = 9, 9', 10, 10', P, P', S, S', T, T5$ only. This procedure follows what is done in $b \to s\ell^+ \ell^-$ transitions.

The matrix elements arising from these effective operators can be classified as either local form factors or nonlocal form factors. Local form factors enter the amplitudes through the hadronic matrix elements of a two-parton current, e.g., from the semileptonic operators or the QED radiative operators $i = 7, 7'$. Nonlocal form factors enter the amplitudes through the time-ordered product of the electromagnetic current with effective operators: the four-quark current-current or QCD penguin operators, and radiative operators with $i = 8, 8'$. In Fig. 1 we provide a schematic overview of the two classes of contributions.

In the case of $\bar{B} \to \pi$ transitions, there exist only three local form factors, which are labeled f_+, f_0, and f_T. Other form factors must vanish due to Lorentz invariance and parity conservation within the strong interaction. The three form factors are defined via:

$$\langle \bar{\pi}(k) | \bar{b} \gamma^\mu d | \bar{B}(p) \rangle = \left[(p+k)^\mu - \frac{M_B^2 - M_\pi^2}{q^2} q^\mu \right] f_+(q^2) + \frac{M_B^2 - M_\pi^2}{q^2} q^\mu f_0(q^2), \tag{2.3}$$

$$\langle \bar{\pi}(k) | \bar{b} \sigma^{\mu\nu} q_\nu d | \bar{B}(p) \rangle = \frac{i}{M_B + M_\pi} [q^2 (p+k)^\mu - (M_B^2 - M_\pi^2) q^\mu] f_T(q^2). \tag{2.4}$$

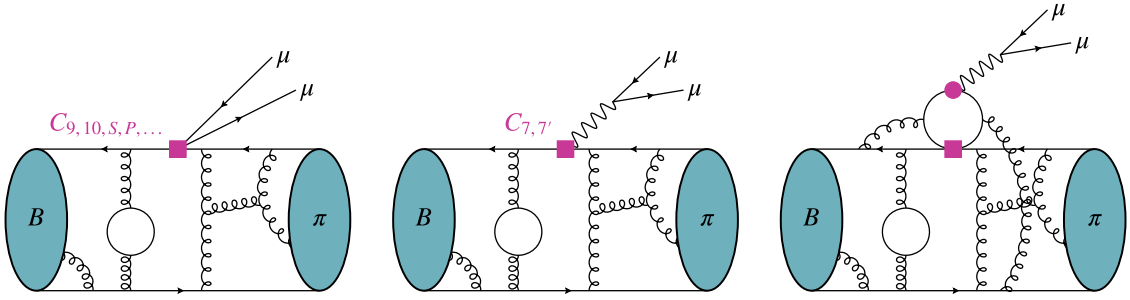

FIG. 1. Schematic overview of the two classes of contributions to $B^\pm \to \pi^\pm \mu^+ \mu^-$ decays. The local contributions are presented in the left and central sketches, and one example of the nonlocal contributions is presented in the right sketch.

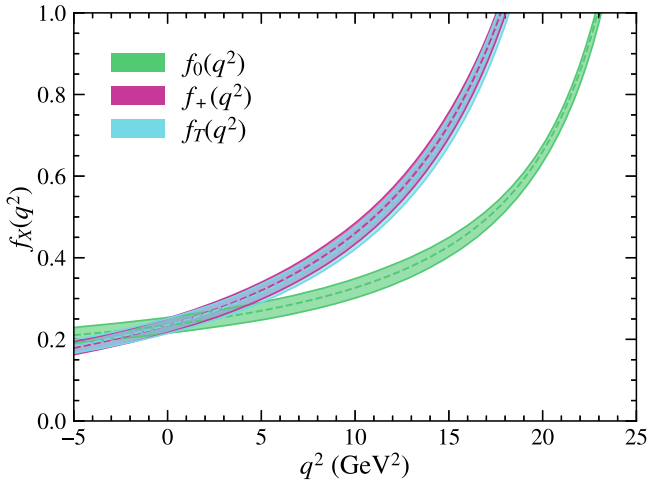

FIG. 2. $\bar{B} \to \pi$ local form factors obtained in Ref. [33] by a combined fit to lattice QCD and light cone sum rule estimates. The bands correspond to the 68% interval.

The form factors are scalar-valued functions of the momentum transfer q^2, which requires some form of parametrization. Here, we use the nominal parametrization and numerical results from Ref. [33]. The parametrization used is based on the original BCL parametrization [34]. The numerical results are obtained from a combined fit to lattice QCD [35–37] and LCSR [33,38,39] inputs. We display these form factor results in Fig. 2.

The Lagrangian density Eq. (2.1) gives further rise to nonlocal contributions, stemming either from the full set of four-quark operators or the radiative operators with $i = 8, 8'$. In the case of $\bar{B} \to \pi$ transitions, there exists only a single Lorentz structure for these nonlocal contributions:

$$\begin{aligned}\mathcal{H}_{\mu}^{(p),B^{\pm}} &= i\int d^4x\, e^{iq\cdot x}\langle\pi(k)|\mathcal{T}\Big\{j_{\mu}^{\mathrm{em}}(x), C_1\mathcal{O}_1^p(0) + C_2\mathcal{O}_2^p(0) \\ &\quad + \sum_{i\in\{3\text{–}6,8,8'\}} C_i\mathcal{O}_i(0)\Big\}|B^{\pm}(p)\rangle \\ &= -\frac{1}{2}[q^2(p+k)^{\mu} - (M_B^2 - M_{\pi}^2)q^{\mu}]\mathcal{H}^{(p),B^{\pm}}(q^2), \\ &\quad (p = u, c). \end{aligned} \tag{2.5}$$

The nonlocal contributions can be recast into a shift to the Wilson coefficient C_9 via:

$$\begin{aligned}\Delta C_9^{B^+}(q^2) &= -16\pi^2\frac{\lambda_u\mathcal{H}^{(u),B^+}(q^2) + \lambda_c\mathcal{H}^{(c),B^+}(q^2)}{\lambda_t f^+(q^2)}, \\ \Delta C_9^{B^-}(q^2) &= -16\pi^2\frac{\lambda_u^*\mathcal{H}^{(u),B^-}(q^2) + \lambda_c^*\mathcal{H}^{(c),B^-}(q^2)}{\lambda_t^* f^+(q^2)}. \end{aligned} \tag{2.6}$$

Due to the CP-violating nature of the weak interaction, we must take care to define such a shift separately for the B^+ and the B^- initial state.

Using the above definitions, the differential decay rate for the $B^{\pm} \to \pi^{\pm}\mu^{+}\mu^{-}$ reads [40]

$$\begin{aligned}&\frac{d\Gamma(B^{\pm} \to \pi^{\pm}\mu^{+}\mu^{-})}{dq^2} \\ &= \frac{G_F^2\alpha^2|V_{tb}V_{td}^*|^2}{2^7\pi^5}|k|\Big\{\frac{2}{3}|k|^2\beta_+^2|C_{10}f_+(q^2)|^2 \\ &\quad + \frac{m_{\mu}^2(M_B^2 - M_{\pi}^2)^2}{q^2M_B^2}|C_{10}f_0(q^2)|^2 \\ &\quad + |k|^2\Big[1 - \frac{1}{3}\beta_+^2\Big]\Big|C_9^{\mathrm{eff},\pm}(q^2)f_+(q^2) \\ &\quad + 2C_7\frac{m_b + m_d}{M_B + M_{\pi}}f_T(q^2)\Big|^2\Big\}, \end{aligned} \tag{2.7}$$

where $q^2 = m_{\mu\mu}^2$ and $|k| = \sqrt{E_{\pi}^2 - M_{\pi}^2}$. This decay rate is defined separately for $B^+ \to \pi^+\mu^+\mu^-$ and $B^- \to \pi^-\mu^+\mu^-$, with each having a unique $C_9^{\mathrm{eff},\pm}$ term defined as follows,

$$C_9^{\mathrm{eff},\pm}(q^2) = |C_9|e^{\pm i\delta_{C_9}} + \Delta C_9^{B^{\pm}}(q^2). \tag{2.8}$$

A. Modeling the nonlocal contributions

In the $q^2 < 0$ region, it is possible to compute the size of the nonlocal contributions to $B^{\pm} \to \pi^{\pm}\mu^{+}\mu^{-}$ transitions using QCD factorization and LCSR. The individual nonlocal components are labeled as follows: factorizable loops $\mathcal{H}_{\mathrm{fact,LO}}^{(p)}$, weak annihilation $\mathcal{H}_{\mathrm{WA}}^{(p)}$, factorizable NLO contributions $\mathcal{H}_{\mathrm{fact,NLO}}^{(p)}$, nonfactorizable soft-gluon contributions $\mathcal{H}_{\mathrm{soft}}^{(p)}$ and $\mathcal{H}_{\mathrm{soft},\mathrm{O}_8}^{(p)}$, and nonfactorizable spectator scattering $\mathcal{H}_{\mathrm{nonf,spect}}^{(p)}$, where the $B^{\pm}$ index is dropped for legibility. The individual components are provided in Sec. 3 of Ref. [41]. These components are summed to compute the full nonlocal contribution as in the following expression,

$$\begin{aligned}\mathcal{H}^{(p)}(q^2) &= \mathcal{H}_{\mathrm{fact,LO}}^{(p)}(q^2) + \mathcal{H}_{\mathrm{WA}}^{(p)}(q^2) + \mathcal{H}_{\mathrm{fact,NLO}}^{(p)}(q^2) \\ &\quad + \mathcal{H}_{\mathrm{soft}}^{(p)}(q^2) + \mathcal{H}_{\mathrm{soft},\mathcal{O}_8}^{(p)}(q^2) + \mathcal{H}_{\mathrm{nonf,spect}}^{(p)}(q^2). \end{aligned} \tag{2.9}$$

To model $\mathcal{H}^{(p),B^{\pm}}(q^2)$ across the full q^2 range, including the physical $q^2 > 0$ region, we employ once-subtracted dispersion relations[1] as in Eq. (41) of Ref. [41]. Combining with Eq. (2.6) results in the following relation,

$$\begin{aligned}\Delta C_9^{B^{\pm}}(q^2) &= \Delta C_9^{B^{\pm}}(q_0^2) + Y_{\rho,\omega}^{B^{\pm}}(q^2) + Y_{\mathrm{LQC}}^{B^{\pm}}(q^2) \\ &\quad + Y_{J/\psi,\psi(2S),\ldots}^{B^{\pm}}(q^2) + Y_{\mathrm{2P},c\bar{c}}^{B^{\pm}}(q^2). \end{aligned} \tag{2.10}$$

[1]We refer to our model as a once-subtracted dispersion relation following the nomenclature used in Refs. [22,41]. However, while our model is inspired by a dispersion relation it does not qualify as one on mathematical grounds, as discussed later in the section.

To ensure the convergence of the dispersive integral for $\mathcal{H}^{(p),B^\pm}(q^2)$, we require one subtraction in the dispersion relation. The emerging subtraction terms are matched to the results of the QCD factorization and LCSR calculations at the subtraction point q_0^2, as originally proposed in Ref. [41]. For this analysis, we choose the subtraction point $q_0^2 = -1.5\ \text{GeV}^2$. Finally, the various $Y^{B^\pm}(q^2)$ terms are the individual components of the nonlocal contributions that will be introduced in the following paragraphs.

Resonances The resonances considered within the full q^2 spectra of $B^\pm \to \pi^\pm\mu^+\mu^-$ decays are the $\rho(770)$, $\omega(782)$, J/ψ, $\psi(2S)$, $\psi(3770)$, $\psi(4040)$, $\psi(4160)$, and $\psi(4415)$. As in Ref. [41], we ignore the presence of the $\phi(1020)$ since its production is either OZI suppressed (in the production through current-current operators) or suppressed by small values of the SM Wilson coefficients (in the production through QCD penguin operators).

Each resonance (V) contribution to $\Delta C_9^{B^\pm}(q^2)$ is described with a relativistic Breit-Wigner distribution as follows,

$$Y_V^{B^\pm}(q^2) = \eta_V^{B^\pm} e^{i\delta_V^{B^\pm}} \frac{(q^2 - q_0^2)}{(m_V^2 - q_0^2)} \frac{m_V \Gamma_{0V}}{(m_V^2 - q^2) - i m_V \Gamma_V(q^2)}. \tag{2.11}$$

Here η_V is the resonance magnitude, δ_V its phase,[2] and $\Gamma_V(q^2)$ the running width,

$$\Gamma_V(q^2) = \frac{p(q^2)}{p(m_V^2)} \frac{m_V}{\sqrt{q^2}} \Gamma_{0V},$$
$$\text{where } p(q^2) = \frac{\sqrt{\lambda(q^2, m_\mu^2, m_\mu^2)}}{2\sqrt{q^2}},$$
$$\text{where } \lambda(A,B,C) = A^2 + B^2 + C^2 - 2(AB + AC + BC). \tag{2.12}$$

The description of the width involves the breakup momentum p both as a function of q^2 and evaluated at $q^2 = m_V^2$. Our choice of the description of the residues in terms of two magnitude and phases, one each for the B^+ and B^- decays, facilitates the description of CP-violation in the decay.

Open charm continuum We jointly model the combination of the nonresonant continuum of open charm states and the contributions due to further broad vector charmonia following the model suggested in Ref. [22]. This model is governed by an overall coupling strength for the modeled two-particle open charm continuum and further includes terms for the S- and P-wave contributions. As for the resonance terms, we choose to describe each coupling in terms of a magnitude η and a phase δ, to facilitate the description of CP-violation in the decay. In contrast to our modeling of the resonances, we choose to use the same coupling strength for both B^+ and B^- decay. The model expression reads:

$$Y^{B^+}_{\text{2P},c\bar{c}}(q^2) = \eta_{\text{2P}} e^{i\delta_{\text{2P}}} \sum_{j=D^*D, D^*D^*, DD} \eta_j e^{i\delta_j} \frac{(q^2 - q_0^2)}{\pi} \times \int_{s_0^j}^{\infty} \frac{ds}{(s - q_0^2)} \frac{\hat{\rho}_j(s)}{(s - q^2)},$$
$$Y^{B^-}_{\text{2P},c\bar{c}}(q^2) = Y^{B^+}_{\text{2P},c\bar{c}}(q^2), \tag{2.13}$$

where $\hat{\rho}_i$ are hadronic spectral densities defined in Ref. [22] and we use the same subtraction point $q_0^2 = -1.5\ \text{GeV}^2$ as before. We fix the magnitudes η_{D^*D}, $\eta_{D^*D^*}$, and η_{DD} of the modeled contributions to unity and fix the phases δ_{D^*D}, $\delta_{D^*D^*}$, and δ_{DD} to zero. In contrast, the "global" parameters η_{2P} and δ_{2P} are allowed to vary in fits to pseudodata.

The joint modeling of the heavy charmonium resonances as one-body intermediate states and the two-particle continuum amplitudes inevitably leads to some double counting and model error. We expect this to be insignificant compared to the statistical uncertainties achievable with the upcoming LHCb datasets. To validate this assumption, we assess the impact of this model choice on the measurement of the Wilson coefficients $\mathcal{C}_9$ and $\mathcal{C}_{10}$ we perform fits to pseudodata generated with the default nonlocal amplitudes, including the ones above the open charm threshold, and fit back with variations of the nonlocal amplitude that involve turning off individual open-charm resonant and two-particle amplitudes. The resulting variations on the extracted values of $\mathcal{C}_9$ and $\mathcal{C}_{10}$ are found to be negligible compared to the statistical precision of any current or future experiment.

Light-quark continuum Finally, we need to consider the nonlocal contribution from the "light-quark" continuum, i.e., the continuum of $\bar{u}u$, $\bar{d}d$, and $\bar{s}s$ states. In a perturbative picture, this contribution arises from weak annihilation and light-quark loop diagrams. This contribution is modeled using the following integral over hadronic spectral densities,

$$Y^{B^\pm}_{\text{LQC}}(q^2) = \sum_{q=u,c} \int_{s_0 \simeq 1.5\ \text{GeV}^2}^{4m_D^2} ds \times \frac{(q^2 - q_0^2)\rho^{(q^\pm)}_{\text{LO}}(s)}{(s - q_0^2)(s - q^2 - i\sqrt{s}\Gamma_{\text{eff}}(s))}, \tag{2.14}$$

where $\rho^{(u)}_{\text{LO}}(s)$, $\rho^{(c)}_{\text{LO}}(s)$, and Γ_{eff} are provided in Eqs. (38) and (39), and in the text of Ref. [41], respectively. Using a duality threshold $s_0 = 1.5\ \text{GeV}^2$ reduces the impact of any potential double counting between the $\rho(770)$ and the $\omega(782)$ and the light-quark continuum. The physical quantities that build up

[2]Contrary to what is done in the description of exclusive $b \to s\mu^+\mu^-$ decays, the phases in our hadronic model for the nonlocal contributions are not strong phases; instead, they are superpositions of two strong phases arising from the two terms and the relative weak phase in Eq. (2.1).

this component are known well enough such that $Y^{B^{\pm}}_{\mathrm{LQC}}(q^2)$ is fixed in the fit.

III. ANALYSIS SETUP

We generate pseudodatasets using the decay rate in Eq. (2.7) and keep the Wilson coefficients set to their SM values. The parameters that describe the local form factors are assigned to the central values obtained in Ref. [33]. The parameters in the description of the nonlocal form factors are instead obtained from a χ^2 fit of our model described in Sec. II A to the theoretical pseudo data points at $q^2 < 0$ computed in Ref. [41]. Our results for the latter parameters are compatible with those of Ref. [41]. We present our results for the nonlocal contributions expressed in terms of the quantity ΔC_9 in Fig. 3.

To ascertain a realistic expected precision on the parameters of interest from the fit to the q^2 spectrum of $B^{\pm} \to \pi^{\pm}\mu^{+}\mu^{-}$ decays, we need to take into account the expected experimental q^2 resolution $R(q^2{}_{\mathrm{reco}}, q^2)$ and the reconstruction efficiency $\varepsilon(q^2)$. We use the experimental q^2 resolution used in the LHCb analysis of $B^{\pm} \to K^{\pm}\mu^{+}\mu^{-}$ decays in Ref. [42]. Our choice is motivated by the expectation that this resolution is close, if not identical, to the LHCb resolution for $B^{\pm} \to \pi^{\pm}\mu^{+}\mu^{-}$ decays. For the reconstruction efficiency, we take the q^2 shape of the efficiency reported in Ref. [42] and extrapolate it linearly to the larger phase space of $B^{\pm} \to \pi^{\pm}\mu^{+}\mu^{-}$ decays. The final signal q^2 model is given by the convolution

$$R(q^2{}_{\mathrm{reco}}, q^2) \otimes \left(\frac{d\Gamma}{dq^2}\varepsilon(q^2)\right), \tag{3.1}$$

which is obtained through a fast Fourier transform.

The signal yield is obtained using the expression

$$N^{B^{\pm}}_{\mathrm{sig}} = \mathcal{L}\alpha N_{B^{\pm}\to J/\psi K^{\pm}} \left|\frac{V_{cd}}{V_{cs}}\right|^2 \frac{\int \frac{d\Gamma(B^{\pm})}{dq^2} dq^2}{\int |Y^{B^{\pm}}_{J/\psi}(q^2)|^2 dq^2}, \tag{3.2}$$

where α is a factor that represents all relative efficiency effects such that the calculated signal yield is compatible with that of the measured yields in different q^2 bins in Ref. [24]. The factor $N_{B^{\pm}\to J/\psi K^{\pm}}$ is the reconstructed yield of $B^{\pm} \to J/\psi(\to \mu^{+}\mu^{-})K^{\pm}$ candidates taken from Ref. [42] that used 3 fb^{-1} of LHCb Run1 data. The ratio of CKM matrix elements converts $N_{B^{\pm}\to J/\psi K^{\pm}}$ to the number of expected $B^{\pm} \to J/\psi K^{\pm}$ decays. The factor $\mathcal{L}$

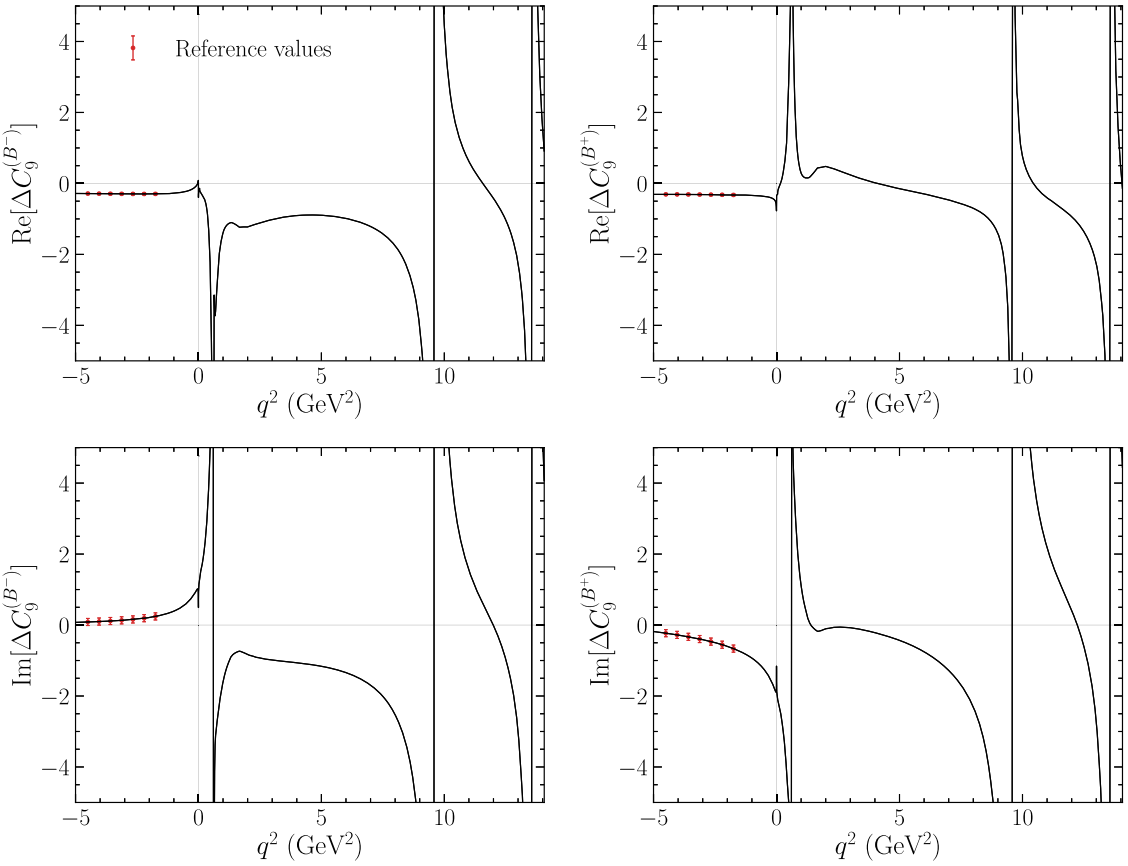

FIG. 3. The model employed for the nonlocal contributions to $B^{\pm} \to \pi^{\pm}\mu^{+}\mu^{-}$, along with the $q^2 < 0$ reference values and introduced in Eq. (3.1).

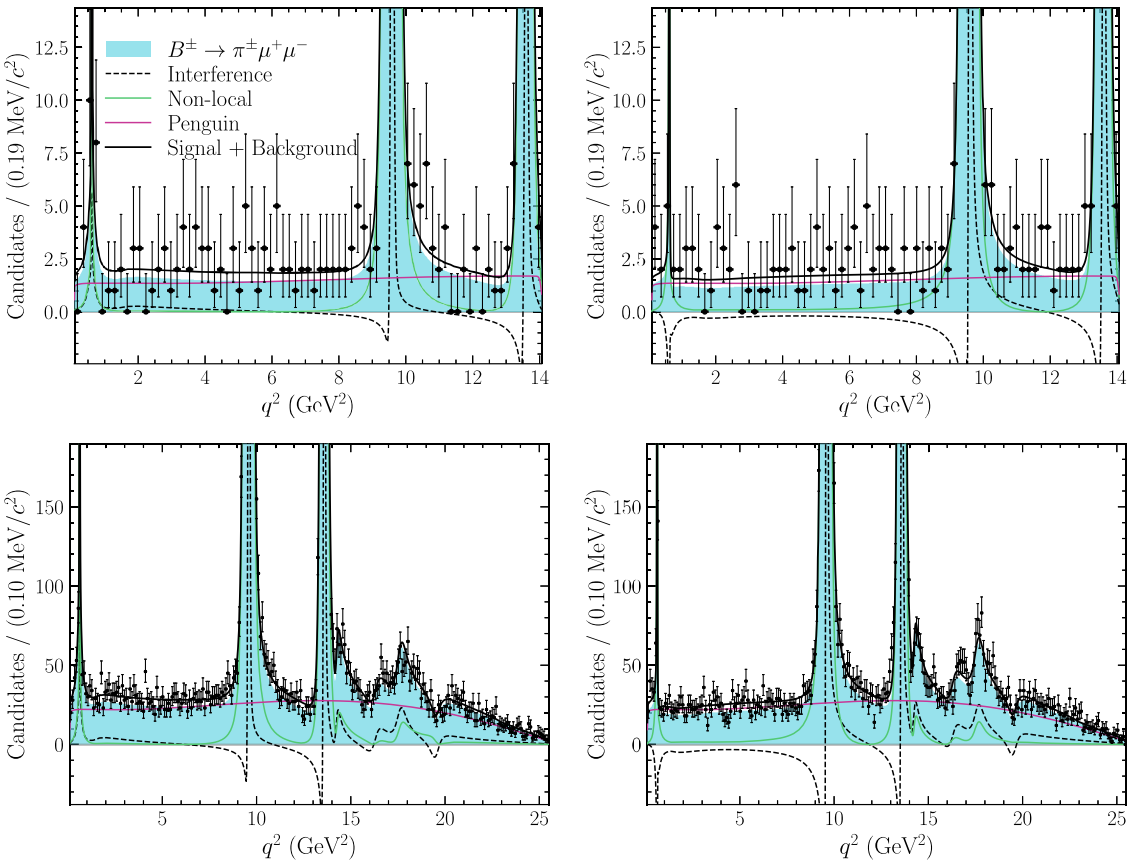

FIG. 4. Pseudodata generated to represent a selected $B^\pm \to \pi^\pm\mu^+\mu^-$ dataset obtained from Run1 + 2 of LHCb data (top) and 300 fb^{-1} (bottom), $B^+ \to \pi^+\mu^+\mu^-$ (left), and $B^- \to \pi^-\mu^+\mu^-$ (right).

scales up the yields from 3 fb^{-1} of LHCb Run1 data to future projections of LHCb integrated luminosities, including the increase in the B-hadron production cross sections coming from the center-of-mass energy changes of the LHC. The factor $\frac{\int \frac{d\Gamma}{dq^2} dq^2}{\int |Y^\pm_{J/\psi}(q^2)|^2 dq^2}$ uses our model of the $B^\pm \to \pi^\pm\mu^+\mu^-$ decay rate to transform the $B^\pm \to J/\psi\pi^\pm$ yield into one across the entire q^2 phase space. Finally, the signal purity is estimated from Fig. 3 of Ref. [24], and the q^2 model of the background is taken from Fig. 3 of Ref. [42] and modeled using a kernel density estimator. Pseudodatasets are generated with a sample size corresponding to that expected in the current LHCb Run1 + 2 dataset (9 fb^{-1}) and future LHCb Upgrades of 23 fb^{-1}, 45 fb^{-1}, and 300 fb^{-1}.

We perform unbinned maximum likelihood fits to these pseudodatasets where the magnitude parameters $\eta^{B^\pm}_{J/\psi}$ and the parameters of the local form factors are fixed in the fit. Fixing these parameters incurs a systematic uncertainty, the size of which we assess in Sec. IV B. In this fit configuration, we measure all the phases, including the phase of C_9, relative to that of C_7, which is fixed in the fit.

Examples of pseudodatasets representing 9 fb^{-1} and 300 fb^{-1} are presented in Fig. 4 along with the model employed in the pseudodataset generation. The nonlocal, penguin, and interference components of the model are shown separately.

A. Constraining the nonlocal contribution

We relate the model of the nonlocal contribution $\Delta C_9^{B^\pm}$, as in Eq. (2.10), to the sum of the various QCD factorization and LCSR predictions at negative q^2 as in Eq. (2.9). This relationship is visualized in Fig. 3 where the red points denote the QCD factorization and LCSR predictions, and the black line is our model of the nonlocal contributions to $B^\pm \to \pi^\pm\mu^+\mu^-$ decays.

We can exploit this relation when fitting our model for the $B^\pm \to \pi^\pm\mu^+\mu^-$ decay rate, Eq. (2.7), to data in the physical $q^2 > 0$ region through the introduction of a multivariate Gaussian factor to the likelihood function. This factor relates our dispersive nonlocal model to the theory reference values computed at different $q^2 < 0$ values, indicated by the red points in Fig. 3. The dimensionality of this multivariate Gaussian constraint is given by the number of negative q^2 points considered multiplied by four.[3]

[3]For the real and imaginary components of the nonlocal amplitude for both B^+ and B^-.

The uncertainties of the reference values and the correlations between these uncertainties need to be taken into account in the multivariate constraint. As Ref. [41] does not provide these correlations, we make the conservative assumption that all the uncertainties used to compute the theory terms are uncorrelated between q^2 points and between real/imaginary B^+/B^- contributions. Assuming the uncertainties between the q^2 points are uncorrelated reduces the statistical power of the constraint.

Constraints are placed on the magnitude parameters of the resonances $V = \rho(770)$, $\omega(782)$, and $\psi(2S)$ using measured central values and uncertainties for the CP-averaged branching fractions of $\mathcal{B}(B \to V(\to \mu^+\mu^-)\pi)$ and of A_{CP}^{V} [43]. These are essential for reliable fit convergence and are employed in all the fits discussed in this paper.

B. Choosing a q^2 range

The region of q^2 above the open-charm threshold is particularly problematic due to the presence of multiple broad overlapping resonances that interfere with nonresonant contributions. With the number of signal decays expected in the existing LHCb Run1 + 2 dataset, it is unfeasible to float all the parameters associated with nonlocal contributions arising from open-charm states. Their impact, however, is subdominant for $q^2 \lesssim 14\ \mathrm{GeV}^2$. This leads us to fix these parameters and to restrict the phase space region for our analysis.

We use the results from the $B^+ \to K^+\mu^+\mu^-$ measurement of Ref. [42] scaled by $|V_{cd}/V_{cs}|$ to fix the residues of the open-charm states. We further limit the phase space to $q^2_{\mathrm{reco}} < 14.06\ \mathrm{GeV}^2$. This cut is motivated by the fact that, taking into account resolution effects, contributions above the $\psi(3770)$ are negligible.

In future datasets, such as those expected by LHCb's planned upgrade, the signal yield will be sufficient to fit the entire q^2 phase space with these nonlocal parameters floating. Therefore, the open charm region is included in the fits to 300 fb^{-1} of pseudodata, as presented in the bottom panels of Fig. 4.

C. Contamination from $B^{\pm} \to K^{\pm}\mu^{+}\mu^{-}$

The decay $B^{\pm} \to K^{\pm}\mu^{+}\mu^{-}$ with a $K^{\pm} \to \pi^{\pm}$ misidentification is a potentially dangerous background to measurements of $B^{\pm} \to \pi^{\pm}\mu^{+}\mu^{-}$ as it is less CKM suppressed than the $B^{\pm} \to \pi^{\pm}\mu^{+}\mu^{-}$ process. However, the binned measurement of the $B^{\pm} \to \pi^{\pm}\mu^{+}\mu^{-}$ decay rate presented in Ref. [24] demonstrated that the $B^{\pm} \to K^{\pm}\mu^{+}\mu^{-}$ background can be brought under control through the use of particle identification information from the ring-imaging Cherenkov systems of LHCb. In this study, we assume the signal purity of a window of ± 40 MeV around the $B^{\pm}$ mass as given in Ref. [24]. However, the $B^{\pm} \to \pi^{\pm}\mu^{+}\mu^{-}$ analysis of Ref. [24] vetoed the regions associated with resonant dimuon contributions from $B^{\pm} \to K^{\pm}\psi(\to \mu^+\mu^-)$ decays, where ψ is J/ψ or $\psi(2S)$. Therefore, our assumed purity of $B^{\pm} \to \pi^{\pm}\mu^{+}\mu^{-}$ decays in the q^2 regions near the large charmonia resonances is not valid. In principle, an experimental analysis that attempts to fit the entire q^2 spectrum of $B^{\pm} \to \pi^{\pm}\mu^{+}\mu^{-}$ decays would have to adopt stricter particle identification criteria to reduce the background from $B^{\pm} \to K^{\pm}\psi(\to \mu^+\mu^-)$ decays down to a controllable level at the expense of signal efficiency. An experimental analysis may need to undertake some optimization of the selection, including a background component for $B^{\pm} \to K^{\pm}\psi(\to \mu^+\mu^-)$ backgrounds in the fitted model and studying the impact on the signal precision. Therefore, dealing with this background is beyond the scope of our study.

IV. EXPERIMENTAL PRECISION AND PROSPECTS

To estimate the expected sensitivity to new physics and understand the impact of the $q^2 < 0$ constraint, we fit generated pseudodatasets with and without the theoretical constraint at $q^2 < 0$ included in the likelihood. Each fit is initialized from multiple starting positions to avoid localized turning points in the likelihood space. The fit result with the largest likelihood is recorded.

A. Fit stability

With the signal yields expected from the 9 fb^{-1} LHCb Run1 + 2 dataset, we find that the best-fit point of a significant fraction of pseudodatasets lies in an unphysical region. The decay rate of Eq. (2.7) is not differentiable with respect to C_{10} in the point $C_{10} = 0$ due to the $|C_{10}|^2$ dependence in the decay rate. As our likelihood minimization relies on gradient descent methods, the algorithm fails when the estimated value of $C_{10} \approx 0$. Reparametrizing the likelihood in terms of $|C_{10}|^2$ (rather than C_{10}), we find the fits to these pseudodatasets converge with negative $|C_{10}|^2$ values, implying an unphysical value for $|C_{10}|$. We, therefore, classify these fits as failed and remove them from our ensembles of pseudo experiments. We report the fraction of successful fits as a function of dataset size for fits with and without the $q^2 < 0$ constraint applied in Table I.

TABLE I. Stability of the fits to pseudo-data. The last column separates fits that do not use theoretical inputs at negative q^2 from those that do.

Size of the dataset	Relative size	Fit success (%)	
		w/o $q^2 < 0$	With $q^2 < 0$
9 fb^{-1}	1	36	78
23 fb^{-1}	2.5	83	94
45 fb^{-1}	5	91	95
300 fb^{-1}	33	100	100

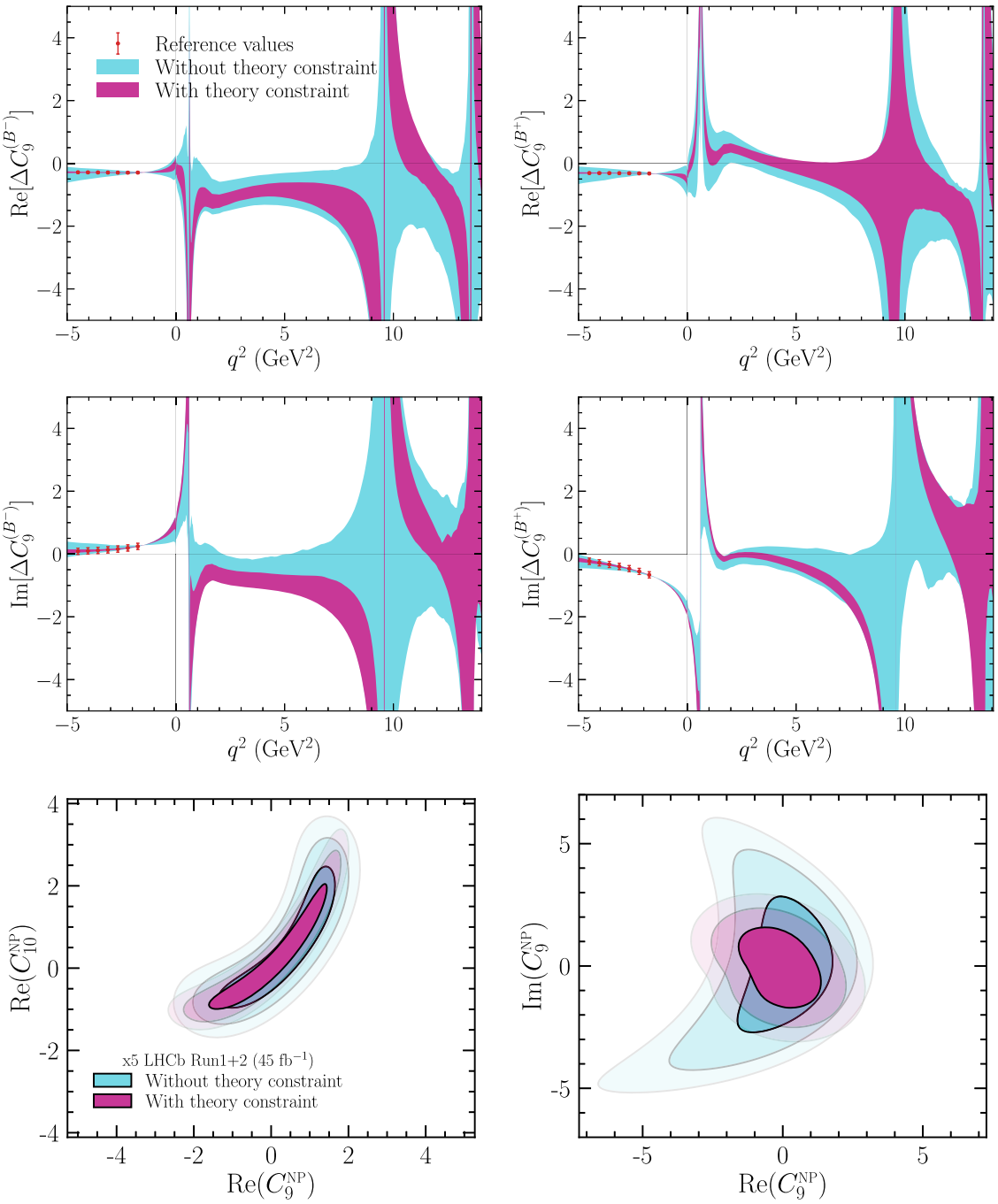

FIG. 5. The statistical sensitivity obtained from fits to pseudodatasets representative of x5 the expected LHCb Run1 + 2 yields showing (top and middle) the 68% intervals for the nonlocal component of $C_9^{\mathrm{eff},\pm}(q^2)$; (bottom) the 68%, 95%, and 99% intervals for the Wilson coefficients $\mathrm{Re}(C_{10}^{\mathrm{NP}})$, $\mathrm{Re}(C_9^{\mathrm{NP}})$, and $\mathrm{Im}(C_9^{\mathrm{NP}})$.

We observe that the success rate of the fits increases by increasing the dataset size or by including the $q^2 < 0$ constraint in the likelihood. For smaller-sized datasets, where the fraction of successful fits is low, imposing some additional assumption on the new physics model, for example, $C_{10}^{\mathrm{NP}} = -C_9^{\mathrm{NP}}$ (where $C_i^{\mathrm{NP}} = C_i - C_i^{\mathrm{SM}}$), improves fit stability at the expense of introducing a model dependence.

B. Assessing sensitivity to new physics

When employing the $q^2 < 0$ constraint, we observe a significant improvement in the statistical precision of the nonlocal contributions, as shown in Fig. 5. This improvement subsequently translates into gains in the statistical precision of the new physics parameters $\mathrm{Re}(C_{10}^{\mathrm{NP}})$, $\mathrm{Re}(C_9^{\mathrm{NP}})$, and $\mathrm{Im}(C_9^{\mathrm{NP}})$. The phases of the resonances

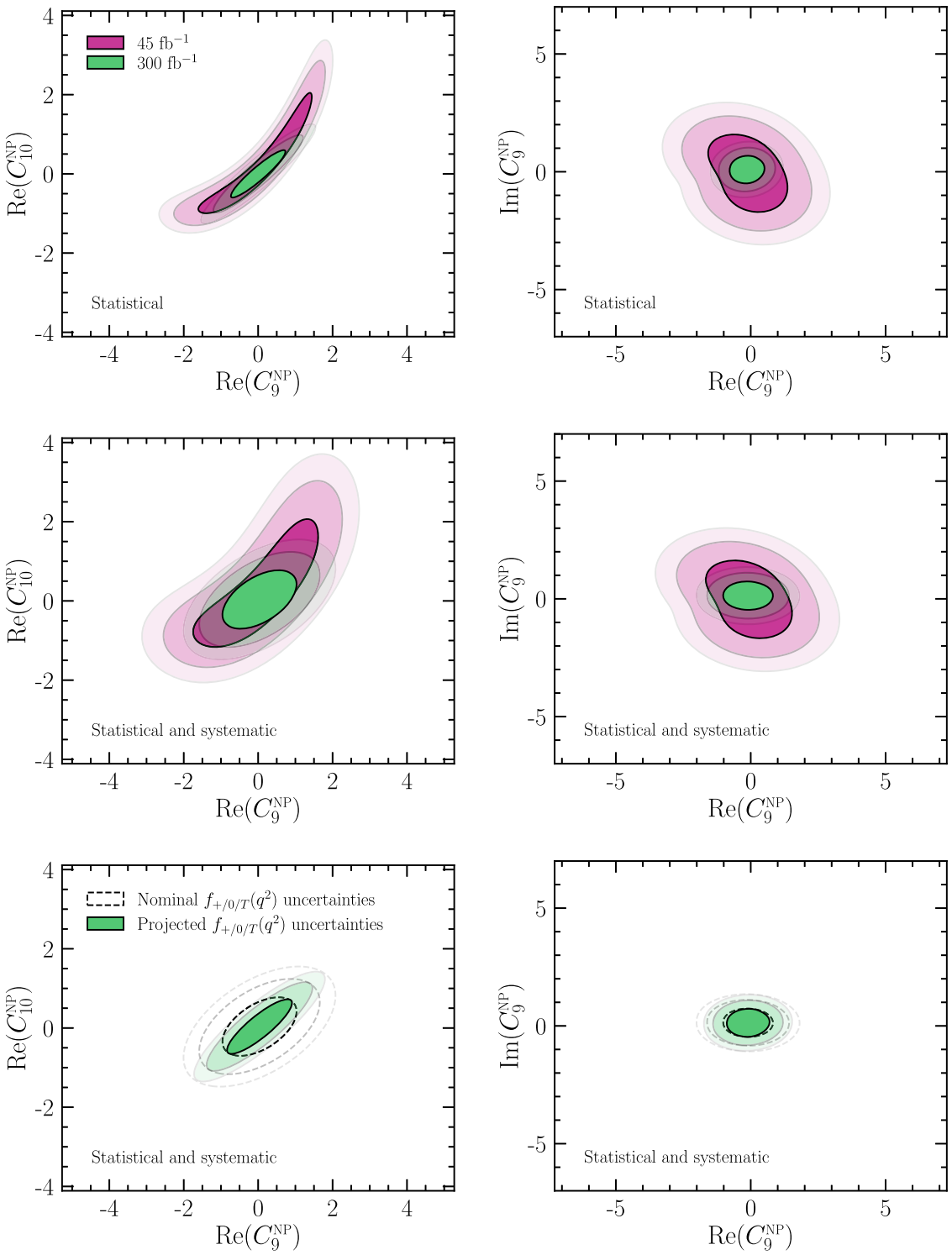

FIG. 6. Two-dimensional intervals on planes of $\mathrm{Re}(C_9^{\mathrm{NP}})$ versus $\mathrm{Re}(C_{10}^{\mathrm{NP}})$ and $\mathrm{Re}(C_9^{\mathrm{NP}})$ versus $\mathrm{Im}(C_9^{\mathrm{NP}})$ showing (top) statistical uncertainty-only intervals (middle) intervals with the inclusion of systematic uncertainties (bottom) a comparison of intervals for 45 fb^{-1} with current local form factor uncertainties (dashed) and with a projected improvement (solid).

and the parameters describing the $Y^{B^{\pm}}_{\mathrm{2P},c\bar{c}}(q^2)$ contributions exhibit significantly reduced uncertainties when employing the $q^2 < 0$ constraint. In contrast, the gains in precision to the magnitude parameters of the resonances are modest as the sensitivity to these parameters is dominated by the prior knowledge of their branching fractions, as mentioned in Sec. III A. Taking the best-fit points of an ensemble of pseudo experiments, we construct confidence intervals that

illustrate the estimated sensitivity to the short-distance parameters $\mathrm{Re}(C_{10}^{\mathrm{NP}})$, $\mathrm{Re}(C_9^{\mathrm{NP}})$, and $\mathrm{Im}(C_9^{\mathrm{NP}})$. These intervals are presented in the lower panels of Fig. 5 for fits to pseudodatasets representing 45 fb^{-1} of LHCb data both with and without the $q^2 < 0$ theory constraint.

The systematic uncertainties that arise from fixing $\eta_{J/\psi}^{B^\pm}$ and the local form factor parameters in the fit are computed and folded into the statistical confidence intervals. These systematic uncertainties are obtained using SM pseudo experiments for 45 fb^{-1} and 300 fb^{-1} scenarios separately. This is done for two reasons. Firstly, the 300 fb^{-1} fits employ the entire q^2 region and float more parameters of the nonlocal model, including those of the open-charm resonances. Secondly, the uncertainties of the $B^\pm \to J/\psi(\to \mu^+\mu^-)\pi^\pm$ branching fractions are scaled for the 300 fb^{-1} scenario according to a projected improvement in precision. The estimated improvement in precision is based on the following assumptions: we assume no improvement in the CP-averaged branching fraction measurement of $B^+ \to J/\psi\pi^\pm$ decays, as it is already systematically limited [4]; we scale the statistical uncertainty of the statistically limited A_{CP} measurement in $B^+ \to J/\psi\pi^\pm$ decays [44] by the expected gain in signal yields at the LHCb experiment; and finally, we assume no improvement in the uncertainty of $\mathcal{B}(J/\psi \to \mu^+\mu^-)$ as it is also systematically dominated [45]. Intervals for the Wilson coefficients $\mathrm{Re}(C_{10}^{\mathrm{NP}})$, $\mathrm{Re}(C_9^{\mathrm{NP}})$, and $\mathrm{Im}(C_9^{\mathrm{NP}})$ both with and without these systematic uncertainties are presented in Fig. 6. These intervals represent the expected sensitivity to these parameters when including the $q^2 < 0$ constraint and are presented for both the 45 fb^{-1} and 300 fb^{-1} scenarios.

The uncertainties of the local form-factor coefficients are the primary source of systematic uncertainty on all the short-distance parameters: $\mathrm{Re}(C_{10}^{\mathrm{NP}})$, $\mathrm{Re}(C_9^{\mathrm{NP}})$, and $\mathrm{Im}(C_9^{\mathrm{NP}})$. We, therefore, stress the importance of reducing form-factor uncertainties alongside the coming increase of signal yield expected from future runs of the LHC. We present an illustrative example to highlight this point. We overlay intervals obtained using smaller form factor uncertainties in the lower panels of Fig. 6. Here, we assume improved calculations could produce uncertainties three times smaller. This would be in line with the improvements achieved for $B \to K^{(*)}$ in Ref. [46]. The improvement in the intervals is significant and brings the result much closer to the statistical-only intervals in the top panels of Fig. 6.

Given that the flavor anomalies could be indicating the presence of large lepton flavour universality violating contributions to C_9^τ, the study of C_9^τ through $b \to d\{e^+e^-, \mu^+\mu^-\}$ transitions is an increasingly interesting subject [47–54]. As demonstrated in Ref. [22], large nonlocal contributions from C_9^τ can be imprinted into the q^2 spectrum of $B^\pm \to K^\pm\mu^+\mu^-$ decays. Larger future datasets of $B^\pm \to \pi^\pm\mu^+\mu^-$ decays could be used to study the q^2 distribution of $B^\pm \to \pi^\pm\mu^+\mu^-$ decays by including a C_9^τ contribution for $\tau\tau$ rescattering to $\mu\mu$. Additionally, with larger datasets, it would be possible to lift the model dependence of the open charm continuum model by floating individual components of the $Y_{\mathrm{2P},c\bar{c}}^{B^\pm}(q^2)$ model or by allowing for CP-violation. Increasing the complexity of the nonlocal model will only increase the relevance of the $q^2 < 0$ constraint. Finally, in the future, it will be possible to fit the $B^\pm \to \pi^\pm\mu^+\mu^-$ decay rate for the presence of new physics with scalar and tensor Wilson coefficients. This would require a 2D fit of q^2 and the lepton helicity angle $\cos(\theta_\ell)$ using the double-differential decay rate [55,56]. Employing the $q^2 < 0$ information will be essential to maximize sensitivity to new physics in all these studies.

V. SUMMARY AND CONCLUSIONS

This paper presents an approach that maximizes the sensitivity of new physics searches in $B^\pm \to \pi^\pm\mu^+\mu^-$ transitions. We employ a dispersive model to perform unbinned maximum likelihood fits to both the measured dimuon q^2 spectrum of $B^\pm \to \pi^\pm\mu^+\mu^-$ decays and to theoretical constraints on the nonlocal contributions at $q^2 < 0$. Our approach ensures that the size and the q^2 dependence of nonlocal contributions to $B^\pm \to \pi^\pm\mu^+\mu^-$ transitions in the $q^2 < 0$ region align with predictions. We perform fits to pseudodatasets and demonstrate the expected sensitivity to CP-violating and CP-conserving contributions for a variety of upcoming datasets. We observe that including the theoretical constraints markedly increases the fit stability and improves the sensitivity to nonlocal parameters and, consequently, to the Wilson coefficients. Variations in the modeling of the nonlocal amplitude above the open-charm threshold were found to have a negligible impact on the extracted values of the Wilson coefficients compared to their statistical precision. We conclude that without increased model dependence, an unbinned analysis of the Run1 + 2 LHCb dataset would be challenging due to poor fit stability. Instead, we present the expected sensitivity for the future scenarios of 45 fb^{-1} and 300 fb^{-1} of LHCb data. We include systematic effects arising from our incomplete knowledge of the $B^\pm \to J/\psi(\to \mu^+\mu^-)\pi^\pm$ branching fractions and local form factors. We find that uncertainties due to the local form factor knowledge currently form the dominant systematic uncertainty. This highlights that improving the precision of local form factors will be an essential step to fully exploit the physics potential of future datasets.

ACKNOWLEDGMENTS

A. M. M. acknowledges support by the UK Science and Technology Facilities Council (Grant No. ST/W000490/1). D. v. D. acknowledges support by the UK Science and Technology Facilities Council (Grants No. ST/V003941/1 and ST/X003167/1).

[1] LHCb Collaboration, Angular analysis and differential branching fraction of the decay $B_s^0 \to \phi\mu^+\mu^-$, J. High Energy Phys. 09 (2015) 179.

[2] LHCb Collaboration, Measurements of the S-wave fraction in $B^0 \to K^+\pi^-\mu^+\mu^-$ decays and the $B^0 \to K^*(892)^0\mu^+\mu^-$ differential branching fraction, J. High Energy Phys. 11 (2016) 047.

[3] LHCb Collaboration, Branching fraction measurements of the rare $B_s^0 \to \phi\mu^+\mu^-$ and $B_s^0 \to f_2'(1525)\mu^+\mu^-$- decays, Phys. Rev. Lett. **127**, 151801 (2021).

[4] BELLE Collaboration, Test of lepton flavor universality and search for lepton flavor violation in $B \to K\ell\ell$ decays, J. High Energy Phys. 03 (2021) 105.

[5] Belle Collaboration, Test of lepton-flavor universality in $B \to K^*\ell^+\ell^-$ decays at Belle, Phys. Rev. Lett. **126**, 161801 (2021).

[6] Belle Collaboration, Lepton-flavor-dependent angular analysis of $B \to K^*\ell^+\ell^-$, Phys. Rev. Lett. **118**, 111801 (2017).

[7] LHCb Collaboration, Angular analysis of the $B^+ \to K^{*+}\mu^+\mu^-$ decay, Phys. Rev. Lett. **126**, 161802 (2021).

[8] LHCb Collaboration, Measurement of CP-averaged observables in the $B^0 \to K^{*0}\mu^+\mu^-$ decay, Phys. Rev. Lett. **125**, 011802 (2020).

[9] LHCb Collaboration, Angular analysis of the rare decay $B_s^0 \to \phi\mu^+\mu^-$, J. High Energy Phys. 11 (2021) 043.

[10] ATLAS Collaboration, Angular analysis of $B_d^0 \to K^*\mu^+\mu^-$ decays in pp collisions at $\sqrt{s} = 8$ TeV with the ATLAS detector, J. High Energy Phys. 10 (2018) 047.

[11] CMS Collaboration, Angular analysis of the decay $B^+ \to \mathrm{K}^*(892)^+\mu^+\mu^-$ in proton-proton collisions at $\sqrt{s} = 8$ TeV, J. High Energy Phys. 04 (2021) 124.

[12] CMS Collaboration, Angular analysis of the decay $B^0 \to K^{*0}\mu^+\mu^-$ from pp collisions at $\sqrt{s} = 8$ TeV, Phys. Lett. B **753**, 424 (2016).

[13] LHCb Collaboration, Measurement of lepton universality parameters in $B^+ \to K^+\ell^+\ell^-$ and $B^0 \to K^{*0}\ell^+\ell^-$ decays, Phys. Rev. D **108**, 032002 (2023).

[14] M. Algueró, A. Biswas, B. Capdevila, S. Descotes-Genon, J. Matias, and M. Novoa-Brunet, To (b)e or not to (b)e: No electrons at LHCb, Eur. Phys. J. C **83**, 648 (2023).

[15] M. Ciuchini, M. Fedele, E. Franco, A. Paul, L. Silvestrini, and M. Valli, Constraints on lepton universality violation from rare B decays, Phys. Rev. D **107**, 055036 (2023).

[16] D. Guadagnoli, C. Normand, S. Simula, and L. Vittorio, Insights on the current semi-leptonic B-decay discrepancies —and how $B_s \to \mu^+\mu^-\gamma$ can help, J. High Energy Phys. 10 (2023) 102.

[17] N. Gubernari, M. Reboud, D. van Dyk, and J. Virto, Improved theory predictions and global analysis of exclusive $b \to s\mu^+\mu^-$ processes, J. High Energy Phys. 09 (2022) 133.

[18] F. Dettori, D. Guadagnoli, and M. Reboud, $B_s^0 \to \mu^+\mu^-\gamma$ from $B_s^0 \to \mu^+\mu^-$, Phys. Lett. B **768**, 163 (2017).

[19] G. Isidori, Z. Polonsky, and A. Tinari, Semi-inclusive $b \to s\bar{\ell}\ell$ transitions at high q^2, Phys. Rev. D **108**, 093008 (2023).

[20] T. Blake, U. Egede, P. Owen, K. A. Petridis, and G. Pomery, An empirical model to determine the hadronic resonance contributions to $\bar{B}^0 \to \bar{K}^{*0}\mu^+\mu^-$ transitions, Eur. Phys. J. C **78**, 453 (2018).

[21] M. Chrzaszcz, A. Mauri, N. Serra, R. Silva Coutinho, and D. van Dyk, Prospects for disentangling long- and short-distance effects in the decays $B \to K^*\mu^+\mu^-$, J. High Energy Phys. 10 (2019) 236.

[22] C. Cornella, G. Isidori, M. König, S. Liechti, P. Owen, and N. Serra, Hunting for $B^+ \to K^+\tau^+\tau^-$ imprints on the $B^+ \to K^+\mu^+\mu^-$ dimuon spectrum, Eur. Phys. J. C **80**, 1095 (2020).

[23] A. Biswas, S. Nandi, S. K. Patra, and I. Ray, Study of the $b \to d\ell\ell$ transitions in the Standard Model and test of new physics sensitivities, J. High Energy Phys. 03 (2023) 247.

[24] LHCb Collaboration, First measurement of the differential branching fraction and CP asymmetry of the $B^{\pm} \to \pi^{\pm}\mu^+\mu^-$ decay, J. High Energy Phys. 10 (2015) 034.

[25] LHCb Collaboration, Evidence for the decay $B_S^0 \to \bar{K}^{*0}\mu^+\mu^-$, J. High Energy Phys. 07 (2018) 020.

[26] LHCb Collaboration, Measurement of the $B_s^0 \to \mu^+\mu^-$ decay properties and search for the $B^0 \to \mu^+\mu^-$ and $B_s^0 \to \mu^+\mu^-\gamma$ decays, Phys. Rev. D **105**, 012010 (2022).

[27] CMS Collaboration, Measurement of the $\mathrm{B}_\mathrm{S}^0 \to \mu^+\mu^-$ decay properties and search for the $\mathrm{B}^0 \to \mu^+\mu^-$ decay in proton-proton collisions at $\sqrt{s} = 13$ TeV, Phys. Lett. B **842**, 137955 (2023).

[28] A. V. Rusov, Probing new physics in $b \to d$ transitions, J. High Energy Phys. 07 (2020) 158.

[29] R. Bause, H. Gisbert, M. Golz, and G. Hiller, Model-independent analysis of $b \to d$ processes, Eur. Phys. J. C **83**, 419 (2023).

[30] M. Bordone, C. Cornella, G. Isidori, and M. König, The LFU ratio R_π in the standard model and beyond, Eur. Phys. J. C **81**, 850 (2021).

[31] C. Bobeth, M. Misiak, and J. Urban, Photonic penguins at two loops and m_t dependence of $BR[B \to X_s l^+ l^-]$, Nucl. Phys. **B574**, 291 (2000).

[32] C. Bobeth, A. J. Buras, F. Kruger, and J. Urban, QCD corrections to $\bar{B} \to X_{d,s}\nu\bar{\nu}$, $\bar{B}_{d,s} \to \ell^+\ell^-$, $K \to \pi\nu\bar{\nu}$ and $K_L \to \mu^+\mu^-$ in the MSSM, Nucl. Phys. **B630**, 87 (2002).

[33] D. Leljak, B. Melić, and D. van Dyk, The $\bar{B} \to \pi$ form factors from QCD and their impact on $|V_{ub}|$, J. High Energy Phys. 07 (2021) 036.

[34] C. Bourrely, I. Caprini, and L. Lellouch, Model-independent description of $B \to \pi\ell\bar{\nu}$ decays and a determination of $|V_{ub}|$, Phys. Rev. D **79**, 013008 (2009).

[35] Fermilab Lattice and MILC Collaborations, $|V_{ub}|$ from $B \to \pi\ell\nu$ decays and $(2+1)$-flavor lattice QCD, Phys. Rev. D **92**, 014024 (2015).

[36] Fermilab Lattice and MILC Collaborations, $B \to \pi\ell\ell$ form factors for new-physics searches from lattice QCD, Phys. Rev. Lett. **115**, 152002 (2015).

[37] J. M. Flynn, T. Izubuchi, T. Kawanai, C. Lehner, A. Soni, R. S. Van de Water, and O. Witzel, $B \to \pi\ell\nu$ and $B_s \to K\ell\nu$ form factors and $|V_{ub}|$ from $2+1$-flavor lattice QCD with domain-wall light quarks and relativistic heavy quarks, Phys. Rev. D **91**, 074510 (2015).

[38] P. Ball and R. Zwicky, New results on $B \to \pi, K, \eta$ decay formfactors from light-cone sum rules, Phys. Rev. D **71**, 014015 (2005).

[39] G. Duplancic, A. Khodjamirian, T. Mannel, B. Melic, and N. Offen, Light-cone sum rules for $B \to \pi$ form factors revisited, J. High Energy Phys. 04 (2008) 014.
[40] A. Ali, A. Y. Parkhomenko, and A. V. Rusov, Precise calculation of the dilepton invariant-mass spectrum and the decay rate in $B^{\pm} \to \pi^{\pm}\mu^{+}\mu^{-}$ in the SM, Phys. Rev. D **89**, 094021 (2014).
[41] C. Hambrock, A. Khodjamirian, and A. Rusov, Hadronic effects and observables in $B \to \pi\ell^{+}\ell^{-}$ decay at large recoil, Phys. Rev. D **92**, 074020 (2015).
[42] LHCb Collaboration, Measurement of the phase difference between short- and long-distance amplitudes in the $B^{+} \to K^{+}\mu^{+}\mu^{-}$ decay, Eur. Phys. J. C **77**, 161 (2017).
[43] Particle Data Group, Review of particle physics, Prog. Theor. Exp. Phys. **2022**, 083C01 (2022).
[44] LHCb Collaboration, Measurement of the ratio of branching fractions and difference in CP asymmetries of the decays $B^{+} \to J/\psi\pi^{+}$ and $B^{+} \to J/\psi K^{+}$, J. High Energy Phys. 03 (2017) 036.
[45] BESIII Collaboration, Precision measurements of $\mathcal{B}[\psi(3686) \to \pi^{+}\pi^{-}J/\psi]$ and $\mathcal{B}[J/\psi \to l^{+}l^{-}]$, Phys. Rev. D **88**, 032007 (2013).
[46] N. Gubernari, M. Reboud, D. van Dyk, and J. Virto, Dispersive analysis of $B \to K^{(*)}$ and $B_s \to \phi$ form factors, J. High Energy Phys. 12 (2023) 153.
[47] C. Bobeth and U. Haisch, New physics in Γ_{12}^{s}: $(\bar{s}b)(\bar{\tau}\tau)$ operators, Acta Phys. Pol. B **44**, 127 (2013).
[48] S. L. Glashow, D. Guadagnoli, and K. Lane, Lepton flavor violation in B decays?, Phys. Rev. Lett. **114**, 091801 (2015).
[49] R. Alonso, B. Grinstein, and J. Martin Camalich, Lepton universality violation and lepton flavor conservation in B-meson decays, J. High Energy Phys. 10 (2015) 184.
[50] R. Barbieri, G. Isidori, A. Pattori, and F. Senia, Anomalies in B-decays and $U(2)$ flavour symmetry, Eur. Phys. J. C **76**, 67 (2016).
[51] A. Crivellin, D. Müller, and T. Ota, Simultaneous explanation of $R(D^{(*)})$ and $b \to s\mu^{+}\mu^{-}$: The last scalar leptoquarks standing, J. High Energy Phys. 09 (2017) 040.
[52] D. Buttazzo, A. Greljo, G. Isidori, and D. Marzocca, B-physics anomalies: A guide to combined explanations, J. High Energy Phys. 11 (2017) 044.
[53] B. Capdevila, A. Crivellin, S. Descotes-Genon, L. Hofer, and J. Matias, Searching for new physics with $b \to s\tau^{+}\tau^{-}$ processes, Phys. Rev. Lett. **120**, 181802 (2018).
[54] M. Bordone, C. Cornella, J. Fuentes-Martín, and G. Isidori, Low-energy signatures of the PS^3 model: From B-physics anomalies to LFV, J. High Energy Phys. 10 (2018) 148.
[55] C. Bobeth, G. Hiller, and G. Piranishvili, Angular distributions of $\bar{B} \to \bar{K}\ell^{+}\ell^{-}$ decays, J. High Energy Phys. 12 (2007) 040.
[56] C. Bobeth, G. Hiller, and D. van Dyk, General analysis of $\bar{B} \to \bar{K}^{(*)}\ell^{+}\ell^{-}$ decays at low recoil, Phys. Rev. D **87**, 034016 (2013).